ELSEVIER

Magnetic Resonance Imaging 21 (2003) 1175–1189

MAGNETIC RESONANCE IMAGING

Real-time MR artifacts filtering during continuous EEG/fMRI acquisition

G. Garreffa[a,b,c], M. Carnì[a,f], G. Gualniera[e], G.B. Ricci[d], L. Bozzao[d], D. De Carli[a,b], P. Morasso[e], P. Pantano[d], C. Colonnese[c], V. Roma[f], B. Maraviglia[a,b,*]

[a]*Department of Physics, University of Rome, La Sapienza, Rome, Italy*
[b]*Enrico Fermi Center, Rome; Istituto Nazionale Fisica Della Materia Uda Roma 1, Rome, Italy*
[c]*Istituto Neurologico Mediterranteo Neuromed Pozzilli, Isernia, Italy*
[d]*Department of Neurological Sciences, University of Rome, La Sapienza, Rome, Italy*
[e]*Department of Informatics, Systems, Telematics, University of Genova, Genova, Italy*
[f]*EBNeuro S.p.A., Florence, Italy*

Received 15 August 2003; received in revised form 22 August 2003; accepted 23 August 2003

Abstract

The purpose of this study was the development of a real-time filtering procedure of MRI artifacts in order to monitor the EEG activity during continuous EEG/fMRI acquisition. The development of a combined EEG and fMRI technique has increased in the past few years. Preliminary "spike-triggered" applications have been possible because in this method, EEG knowledge was only necessary to identify a trigger signal to start a delayed fMRI acquisition. In this way, the two methods were used together but in an interleaved manner. In real simultaneous applications, like event-related fMRI study, artifacts induced by MRI events on EEG traces represent a substantial obstacle for a right analysis. Up until now, the methods proposed to solve this problem are mainly based on procedures to remove post-processing artifacts without the possibility to control electrophysiological behavior of the patient during fMRI scan. Moreover, these methods are not characterized by a strong "prior knowledge" of the artifact, which is an imperative condition to avoid any loss of information on the physiological signals recovered after filtering. In this work, we present a new method to perform simultaneous EEG/fMRI study with real-time artifacts filtering characterized by a procedure based on a preliminary analytical study of EPI sequence parameters-related EEG-artifact shapes. Standard EEG equipment was modified in order to work properly during ultra-fast MRI acquisitions. Changes included: high-performance acquisition device; electrodes/cap/wires/cables materials and geometric design; shielding box for EEG signal receiver; optical fiber link; and software. The effects of the RF pulse and time-varying magnetic fields were minimized by using a correct head cap wires-locked environment montage and then removed during EEG/fMRI acquisition with a subtraction algorithm that takes in account the most significant EPI sequence parameters. The on-line method also allows a further post-processing utilization.

Keywords: Functional MRI; Electroencephalograph (EEG); Real-time filtering

1. Introduction

Functional MRI allows the high spatial resolution of MR imaging and the possibility to spatially detect changes of tissue oxygenation and perfusion induced by neuronal activation to be combined in one technique . Changes in blood oxygenation induce changes in MR signal (BOLD, Blood Oxygen Level Dependent) that can be detected with a resolution of a few millimeters and a temporal resolution of a few seconds. These characteristics are complementary to the electrophysiologic methods that have a higher temporal but lower spatial resolution. It is therefore clear that the integration of these two noninvasive methods may provide an accurate investigation of brain function. The main application of the combined techniques is represented by the identification of the cortical area associated with neuronal activity. Warach et al. (1996) [1] first demonstrated the clinical applicability of EEG-triggered fMRI by using EEG equipment specifically designed for recording during MR acquisition [2]. However, they did not address the pulse artifact problem. They observed an artifact synchronized with cardiac activity (ballistocardiogram). According to

* Corresponding author. Tel.: +39-0649913473; fax: +39-0649913484.
E-mail address: bruno.maraviglia@roma1.infn.it (B. Maraviglia).

0730-725X/03/$ – see front matter
doi:10.1016/j.mri.2003.08.019

Allen et al. [3], the pulse artifact is induced by blood flow inside the head, normal to the static magnetic field. Initially, this interaction was virtually impossible to eliminate, and the authors showed that a simple adaptive subtraction algorithm can partly solve the problem [4,5]; instead, it is possible to reduce this cardiac activity effect simply through an opportune cable montage and patient head-lock protocol.

Concerning EEG signal alterations due to the gradients (time-varying magnetic fields), Ives et al. [2] and Huang-Hellinger et al. [6] observed that they induce an electromotive force (EMF) in each apparent wire loop perpendicular to the gradient field direction, which is proportional to the cross sectional area of the wire loop and to the slew rate of the gradients.

When wires and electrodes of an EEG device are placed inside the MR scanner, the fast varying gradient fields and the radio-frequency pulses during MRI scan induce a very intense electric noise that obscures the EEG signal. The basic idea of our method is a detailed analysis of the electromagnetic interference in the shape and in space-temporal features. Exact effects estimation of EPI sequence parameters into the raw EEG data gives us the possibility to identify an analytical expression of "artifacts function" that represents a reference (template) for filtering and also to find "endogenous" trigger events. Indeed, we use an internal peak detection algorithm that matches two discrimination criteria to evaluate MRI artifact peaks within the EEG signal: the first and most simple criterion checks signal amplitude, the second one takes into account the timing.

2. Materials and methods

Experimental steps to develop our real-time filtering procedure are described as follows:

1. Standard EEG equipment was modified to work properly during fMRI acquisitions.
2. Detailed EEG-artifact shapes analysis was performed to identify principal relations with EPI sequence parameters commonly used for these studies.
3. A specific algorithm was implemented in order to remove on-line pulse sequence artifacts from EEG without affecting its quality. The software (initially developed in Matlab 6.1 environment and then in C^{++} programming language using Borland C^{++} Builder) is characterized by an interface for loading of EPI sequence parameters.

We investigated the artifact features; this study is barely reported in the literature. About electromagnetic interference that entirely obscures the EEG during scanning, we know both the frequency spectrum and the artifact shape that is closely linked with the most significant EPI sequence parameters. A detailed analysis of RF (radio frequency) and gradient artifact allows us to remove them through an on-line "sample by sample" subtraction. Preliminary results prove that our filtering method assures good EEG quality; our conclusions open an important scene in the use of this new simultaneous EEG/fMRI.

Estimated maximum gradient artifacts amplitude is of about a few tens of millivolts [7–9] (more precisely 12 mV for EEG signals and 120 mV for ECG signal); thus exceeding a standard EEG amplifier range (a diagnostic EEG study is normally recorded with a resolution of a few μV). Therefore, after a preliminary study based on geometrical considerations, we were able to reduce preventively the artifacts' intensity [10]. Our EEG equipment is able to record with up to 32 kHz sampling rate and up to $\pm$65.5 mV dynamic range. For our study, the amplifier was set at 4 kHz sampling rate, which allows a suitable time resolution to pick up the switching effect of the readout gradient in the high slew rate condition, and the EEG dynamic range of $\pm$65.5 mV to prevent that MRI artifact waveforms saturate the EEG/ECG.

A standard portable 40-channel digital EEG amplifier BE/Mizar (EBNeuro S.p.A., Florence, Italy) was adapted to operate inside the MR room. Conic Ag-AgCl electrodes prearranged into a cap of amagnetic material were filled with conductive gel [11]. The EEG device inside a shielded box amplifies the signal and performs A/D conversion. The digital signal is then transferred, via an optical fiber connection, to the host computer outside the magnet room for demultiplexing, data acquisition, processing, and storage.

2.1. EEG-artifact shapes analysis

Simultaneous EEG and EPI acquisitions were performed by means of 1.5 T MR scanner Intera (Philips Medical Systems, Nederland) at the Neurologic Sciences Department of University of Rome, La Sapienza, with gradients amplitude 30 mT/m and slew rate 150 T/m/s.

On-line filtering procedure was applied in biologic phantom (a melon) and in humans: 3 healthy volunteers all males age ranging 25-30 years, and 3 epileptic patients: 1 female and 2 males age ranging 30–60 years.

The approval of the local ethics committee was obtained for all EEG recordings during MRI. All subjects gave their informed, written consent for the study. EPI (Echo Planar Imaging) images were acquired by single shot pulse sequence with the following parameters: TE 60 ms, FOV 24 cm, flip angle 90°, matrix 64 $\times$ 64, 18 contiguous slices with 5 mm thickness.

Continuous fMRI acquisition method was applied with 200 volumes, each one consisting of 18 slices with a repetition delay of 3 s for a total scan time of 10 min. The effects of principal sequence parameters are shown in Fig. 1.

Main dominant frequencies carry out from gradient switching events (see Fig. 2) and from slice timing vs. TR (see Fig. 7C).

Artifact shapes analysis allows us to identify most significative parameters related to gradient-EPI sequence. Temporal determination of the recurrent interference is car-

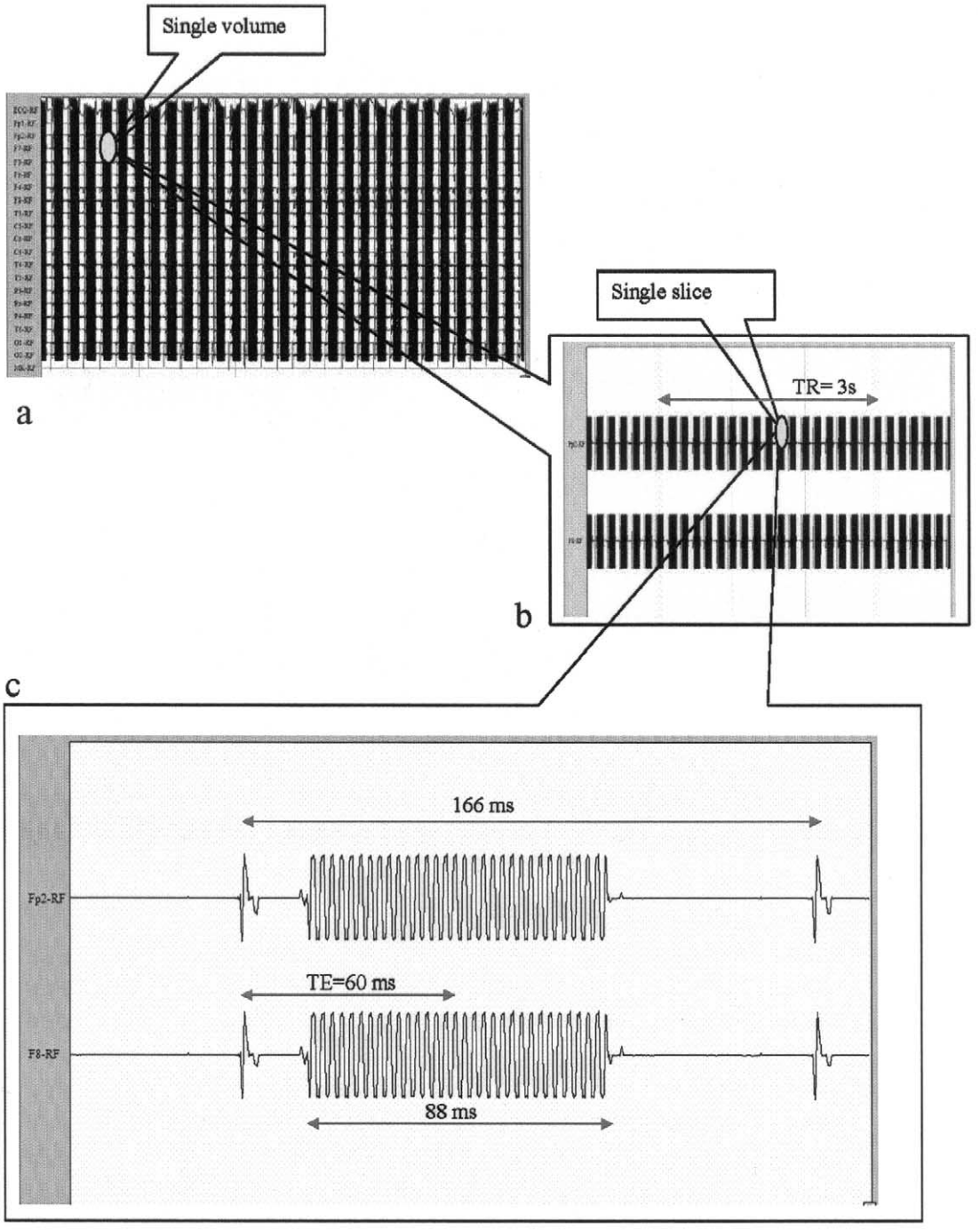

Fig. 1. (A) EEG recorded during EPI acquisition. (B) Enlargement of two channels: the EEG length, concerning 18 slices (1 volume) is equal to TR = 3 s. (C) Single EPI slice artifact events on two EEG channels. In this enlargement, the following are identifiable: slice acquisition time (TR/number of slices: 3s/18 ≈ 166 ms), echo time TE = 60 ms that elapses between RF pulse and the half readout gradient train (88 ms, lower slew rate).

ried out on the EEG-acquired simultaneously with fMRI. It is possible to recognize: low frequency modulation (shape) of RF pulse and slice selection gradient in overlapping manner; alternate lobes of frequency-encoding gradient (the effects of phase encoding gradient are negligible); echo time (which elapses between RF pulse and the middle point in the period of gradient frequency encoding expression); slice acquisition time (TR/number of slices); and other secondary events.

Now we show in details the EEG recorded events inside the MRI scanner during the EPI sequence and the features of induced artifact on the EEG. When the gradients work with high slew rate the encoding period lasts 40 ms while extend up to to 88 ms when lower slew rate is setting (Fig. 1c).

The large artifact called ballistocardiogram is correlated to the current, induced by a wire-like BLOOD movement in

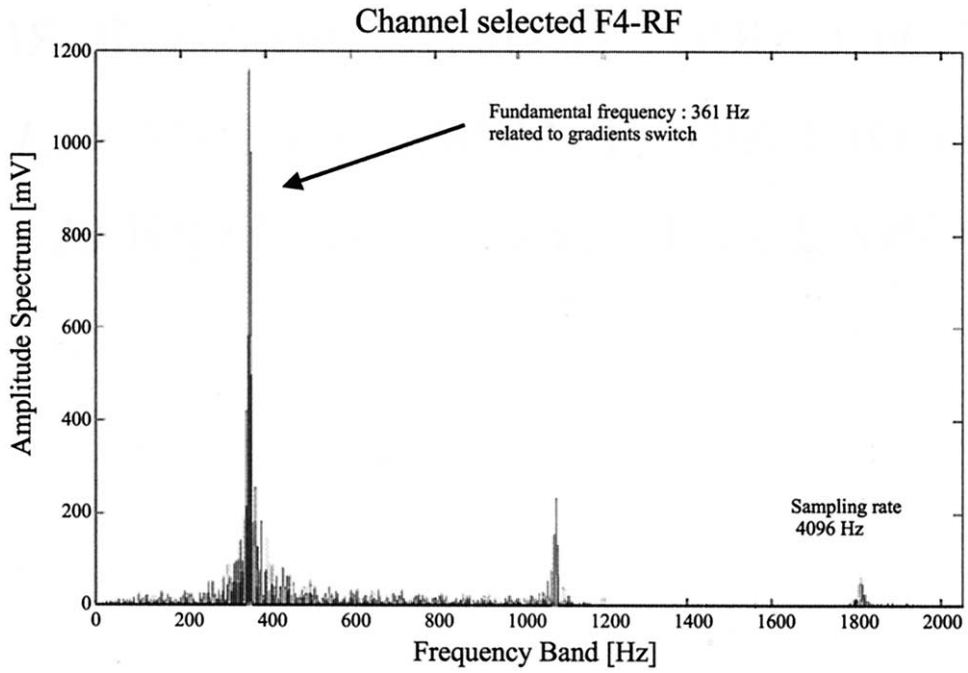

Fig. 2. Main dominant frequencies carry out from gradient switching events.

a magnetic field [3]. This artifact is originated by the slight micromovements of the head due to heartbeat and originate potentials that are sometimes higher than the EEG amplitude. Several methods were proposed to reduce this artifact: by using the spatial properties of the bipolar montage; moreover, cardiac pulse interference can significantly be reduced by a suitable wire setting patient head locking.

2.2. Artifact filtering algorithm

The features of EEG recorded inside the MRI scanner during the EPI sequence were used, in order to consider the whole magnetic artifact interferences on the EEG traces as evoked responses due to a specified "stimulation." For this reasons, the RF pulse and gradient field artifacts were detected, evaluated, and then computed with a standard evoked potential methodic, considering **x(t)** as raw continuous signal acquired by the EEG amplifier.

Two fundamental hypothesis were used. The first one considers **x(t)** as a set of uncorrelated components: the EEG basal activity **eeg(t),** the instrumental noise **n(t)**, and the EPI-evoked response **epi(t)**:

$$x(t) = eeg(t) + n(t) + epi(t) \tag{1}$$

The second one assumes that **eeg(t)** and **n(t)** have zero mean. The EPI signal averaging procedure was briefly articulated in the following steps:

- Applying *M* EPI dynamic stimuli, and record resulting *M* responses;
- Aligning *M* responses to form an ensemble with each response EPI aligned in time;
- Averaging across all responses in the ensemble to get the EPI estimate.

We assume that each response (with **N** samples length corresponding to the duration of each EPI dynamic) was computed by **M** averages:

$$\begin{aligned} x_i(t) &= [x_{i,1}(t), x_{i,2}(t),\ldots,x_{i,N}(t)] \\ &= eeg_i(t) + n_i(t) + epi_i(t), \\ i &= 1,\ldots,M \end{aligned} \tag{2}$$

$$\begin{aligned} x_{avg}(t) &= \frac{1}{M}\sum_{i=1}^{M} x_i(t),\ \frac{1}{M}\sum_{i=1}^{M} x_i(t) = \frac{1}{M} \\ &\cdot \left(\sum_{i=1}^{M} eeg_i(t) + \sum_{i=1}^{M} n_i(t) + \sum_{i=1}^{M} epi_i(t) \right) \end{aligned} \tag{3}$$

$$x_{avg}(t) = eeg_{avg}(t) + n_{avg}(t) + epi_{avg}(t) \tag{4}$$

After M averages $eeg_{avg}(t) \to 0$ and $n_{avg}(t) \to 0$

$$x_{avg}(t) \cong epi_{avg}(t) \tag{5}$$

In this way, the EPI synchronously averaged EEG is an estimate of the average waveform of the whole EPI interference (RF pulses and gradient fields) in the EEG channels. In other words, the overall computational process comprises the following basic operations (Fig. 3):

1. Evaluation of the EPI sequence information into the EEG raw data and subsequently EPI event trigger detection;

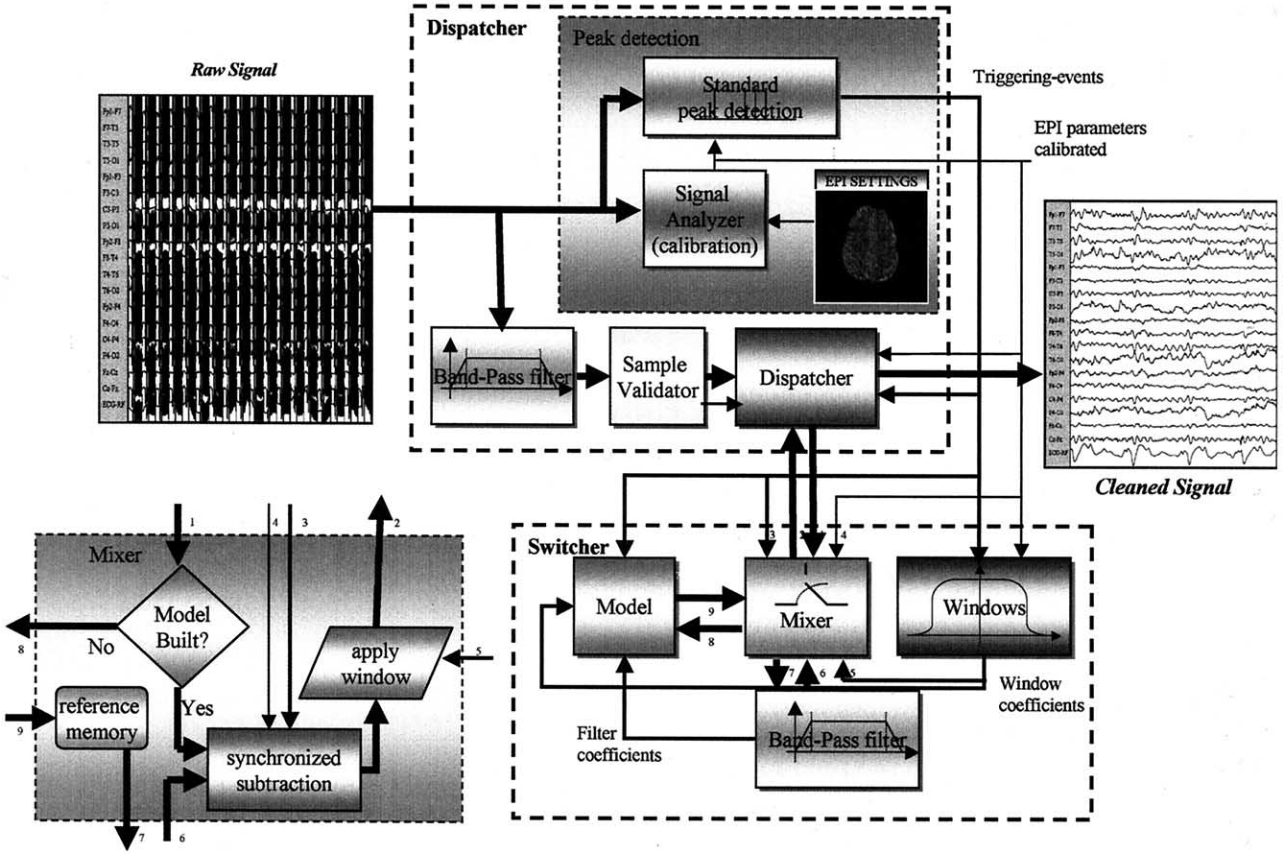

Fig. 3. Block scheme of real-time filter algorithm.

2. Computation of the artificial reference artifact model; and
3. Synchronized interference cancellation by zero-phase band pass filtering, subtraction and final appropriate windowing application.

The filtering algorithm consists of four main steps:

1. First useful MRI sequence scanning;
2. Filter calibration;
3. Artifact model creation; and
4. Cleaning sequence.

The filter, when activated, starts in a *wating mode*, rejecting any event not concerning dynamic measurements (for instance, scanner calibration like dummy or reference scan). Any valid (discerned by amplitude and waveform) MRI sequence will wake up filtering algorithm.

When EPI sequence (*dynamic*) runs, the filter enters in *calibration mode*, and here only 48 s are needed (depending of fMRI parameters setting) to build a robust dynamic model where *pre-delay*, *post-delay* and *inter-peak delay* are measured and averaged to compute scanner specific best settings (Fig. 4). Our study protocol obviously takes in account this silent phase, and co-registration starts when the filter acts in real-time and EEG traces appear cleaned (i.e., 48 s after dynamic EPI scan start).

Moreover, mean signal amplitude will be used to estimate appropriately peak detection threshold.

Artifact model (*model*) is built by averaging a suitable

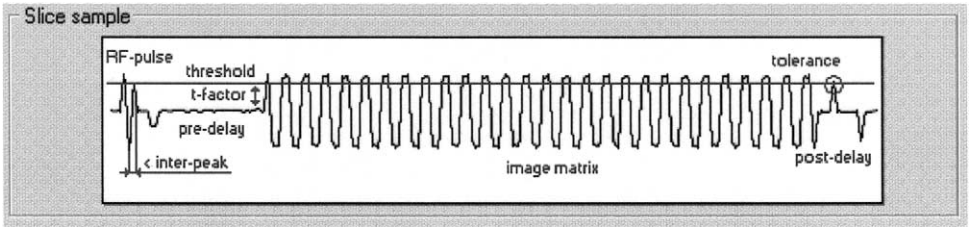

Fig. 4. Particular of a slice sample when specified measures, each related to a specific label, are applied for the slice events, and used for a dedicated peak detection interface algorithm.

number of dynamics: in this way the "background" EEG signal tends to zero and what's left is the MRI artifact. According to filter settings, a window and a band-pass filter may be applied to model. A peak detection algorithm, to find peaks, slices and dynamics, processes each sample (which may be cleaned with additional low-pass and smoothing filters to make peak detection work easy). Peak detection results are used to synchronize raw data (the "dirty" signal) with artifact model.

Each raw sample is associated with the corresponding (in time) sample in the model; cleaned signal is the difference between raw sample and model. Empiric tests demonstrate that a band-pass filter, applied to raw signal before subtraction, dramatically increases filter quality.

Default settings provide a zero-phase 10^{th} order Butterworth low-pass filter pointed to 70 Hz but they can be changed according to user's preferences. Additional filters may be applied: windows (best results with raised cosine), notch (applicable to raw signal before and after peak detection and to cleaned signal) and a simple de-noiser (for Gaussian white noise).

The computation path seen above isn't so easy: each action must be fast enough to guarantee real-time cleaning, to check signal quality, and last but not least, to be adaptable to a wide range of MRI scanners. These goals are reached granting a wide range of options to customize filter behavior.

2.3. Peak detection

Peak detection has a thankless task: to find peaks and to recognize dynamics and slices start points (setting apart noise and spurious peaks). Specific filters (such as a 5^{th} order low-pass Butterworth filter and a smoothing algorithm) can be used and they would be applied to peak detection data only. To reach goals and keep filter flexible two peak detection algorithms are provided and can be combined together:

1. Threshold: a sample's virtually considered a potential peak if its amplitude exceeds a given threshold (estimated at the calibration step).
2. Time and position: This set of rules is applied to peaks (validated by previous threshold rule), and aims to validate peak by position and to collocate them in the dynamic:

Potential peaks are thinned out measuring their distance from most recent one. This to avoid a long peak (which "occupies" a lot of near samples) to be considered as a set of peaks.

Time and position (of the peak) are used to match its right position, making possible to setting apart spurious peaks because they "don't happen" at the right moment.

The *virtual dynamic* used here for comparison purposes is a pulse train in this sequence:

RF pulse;
Clean signal (called pre-delay);
n/2 pulses (where *n* is the number of image pixels);
Clean signal (called post-delay); and
Repeated *s* times (where *s* is the number of slices per dynamic).

Each dynamic can be compared to this ideal dynamic. Counting each slice (RF pulses with which each slice starts), peak detection establishes dynamic edges.

Of course, each channel has its own peak detection with its private threshold (time settings are shared). When a peak is judged to be valid in a given number of channels in the same time, this is then considered a valid peak.

2.4. Automatic calibration

Parameters (threshold and time settings) are critical; in order to always obtain the finest results without the need to involve an excessive effort from the users side, an automatic calibration algorithm is provided. Few dynamics are analyzed (starting with default parameters) to collect real values.

2.5. Model creation

By collecting each sample and averaging them by position (Fig. 3), we obtain a model of the artifact. Instead of computing the length of the model, the length of the first dynamic is assumed as valid. Subsequent dynamics will be stretched or reduced to this size. Longer dynamics will be chopped, reducing their post-delay (in other words cutting off useless samples: they'll be zeroes).

After the model is built, a window may be applied to soften edges. The same window will be applied to raw signal too (of course because model will be subtracted to raw signal!). As told, a band-pass filter may be applied to improve filter quality: identical filter applied to raw signal should be applied to model too, but best results oblige to apply it only when the model is built and averaged.

2.6. The cleaning algorithm

A large number of cleaning algorithms can be used: a simple (synchronized) subtraction allows operating in real–time with a good signal quality. An adaptive Schur–Levinson algorithm [12] (which uses Toeplits equation solving) is used too but it needs fast computers (of course for off-line purposes, speed doesn't matter). The filter "core" is really simple; the signal is cleaned with few actions:

A band-pass filter is applied to raw signal (optionally);
The model is subtracted from raw signal; and
A window is applied to cleaned signal (optionally).

These actions are performed for each sample using peak detection results to keep blocks synchronized.

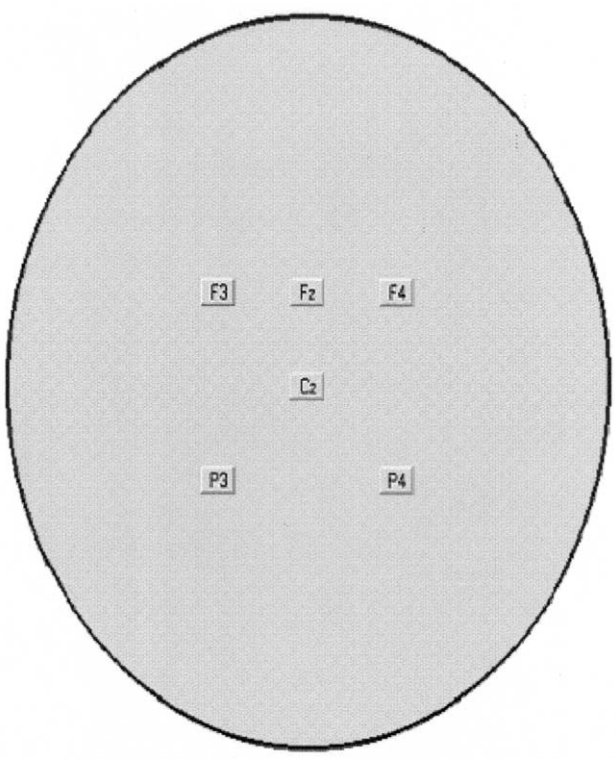

Fig. 5. Particular of a biologic phantom shape of wave, in which are shown the correct location (based on a 10-20 system) of the electrodes used for the experimental registration.

A *smart mixer* option can be enabled to subtract only compatible values. If amplitude of the cleaned signal is greater than model amplitude or if it is too big to be an EEG signal then, maybe, model shouldn't be subtracted from raw signal. This feature may avoid noise near dynamic edges.

Filter is fast enough to ensure real-time cleaning with standard computers (test PC was a Pentium III 800 MHz, 128 Mb RAM). At 4 kHz sampling frequency, the processing time is less than 0.244 ms for one sample. Filter, in the worst case, consumes 0.100 ms/sample. Better case was around 0.01/0.015 ms/sample. Speed can be improved, but at a sampling rate of 8 kHz real-time is still guaranteed. Buffers and filter optimizations (or faster computers) will move sampling limit to 32 kHz and over.

3. Results

A yellow melon was initially studied, like a biologic phantom (Fig. 5), in order to verify the effective contribution (both in time and frequency domain) of the only EPI sequence inside the MR scanner in a simultaneous electrical signal/fMRI acquisition.

The initial hypothesis was to completely recognize the shape of this artifact and to evaluate this one as an uncorrelated information respect to the standard basic noise of this phantom.

A 10-20 system configured head cap was used on the melon, and this "virtual patient" was accurately placed inside the MR scanner, electrical activity was acquired in different MR situations.

A limited number of electrodes was placed on the melon with respect to the standard 10-20 EEG system (which well represent the axial and lateral positions of the head, and where the contribution of the gradient, static and RF fields are the supposed representative), and then acquired for this purpose: F3, Fz, F4, Cz, P3, P4.

Our standard measure protocol for each measure was:

1. Up to 2 min recording inside the MR scanner, after the correct positioning of the phantom and pre scan loading sequence, in absence of the EPI scan (Fig. 6A);
2. From 30 to 100 volumes EPI sequence recording: other two fundamental effects was evidenced, one strictly related to the RF pulse and the last to the gradient fields (Fig. 6C);
3. Up to 2 min of recording inside the MR scanner after EPI protocol scanning. (Fig. 6B).

An accurate study of the biologic phantom recordings evidenced that the morphology of the noise before and after the EPI scan reports the same features both in time and frequency domain, in particular the amplitude spectrum of the channels acquired was computed in a restricted band of the standard EEG signal bandwidth (0-24 Hz respect to 0-32 Hz). We found that the percent variation of the energy of the entire band considered was more or less 9%, so there is no significative variability of information in these two cases (see Table 1).

$$\text{Percent Variation function: } \mathbf{Vp}_{\text{band}}\% = \text{abs}((\mathbf{before}_{\text{band}} - \mathbf{after}_{\text{band}})/\mathbf{before}_{\text{band}}) *100.$$

By using these positives results, we considered that it is possible to study the nature of all artifacts due to the magnetic field in order to obtain similar results when the EPI sequence started. All considerations about the algorithm were reported in another section of this article.

After this, good results were obtained with the adaptive filter, and was found that all features in time and frequency domain of the electrical signals acquired on the biologic phantom does not exceed out of the variability range of the "Before" and "After" cases. (Fig. 6D) note that for each cleaned channel is possible to see the starting point of the volumes (spikes) that are visible because of we have not applied a raised cosine windowing function just to leave visible a temporal volume markers.

In particular the amplitude spectrum for each channel acquired (comparable like 1/Frequency hyperbolic function) was found before, after and also during the sequence (Fig. 7A, B, and D).

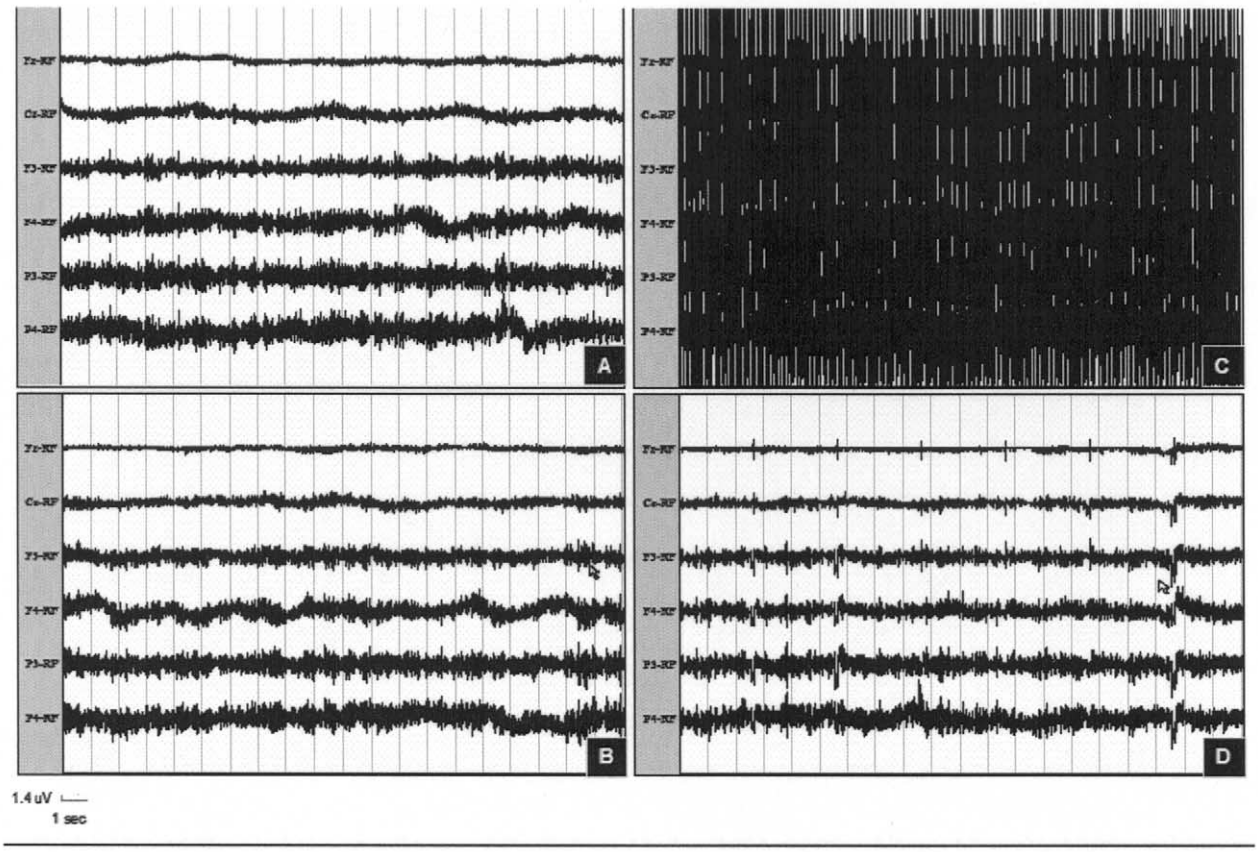

Fig. 6. Twenty-second recording of a biologic phantom in four different cases (0.30 s Time Costant, 70 Hz Low Pass filter, 50 Hz Notch enabled). (A) Before EPI sequence (noise with only static magnetic field effect). (B) After EPI sequence (noise with only static magnetic field effect). (C) During EPI sequence (noise with gradients and static magnetic field, RF pulse effects). (D) During EPI sequence with adaptive filtering.

It is interesting to note that it's possible to consider the amplitude spectrum computed during the EPI sequence like the linear combination of the hyperbolic noise shape plus the repetitive pulse artifact due to all magnetic fields (Fig, 7C).

Similar values were discovered computing the percent variation of the energy of the entire band between the cleaned signal and the average of the spectrum before and after the EPI sequence: more or less 9% (Table 2).

Percent variation function: $Vp_{band}\%$

$$= \text{abs}((\text{cleaned}_{band} - \text{average}(\mathbf{before}_{band}, \mathbf{after}_{band})/\mathbf{cleaned}_{band})*100.$$

The real-time filtering allows us to directly monitor the EEG and the patient behavior during the EPI acquisition. In particular, this becomes useful when the patient is very anxious and tense, and the EEG even with rich epileptic

Table 1
Percent variation for each channel: biological phantom before and after EPI sequence

Band [Hz]	F3	Fz	F4	Cz	P3	P4
Delta [0–4]	7.403651	0.42283	8.8525	14.40678	12.59755	19.0141
Theta [4–8]	8.22762	11.96676	13.9739	0.1912	11.97917	15.1242
Alpha [8–12]	18.18182	13.83648	8.629	13.3048	7.823129	4.42478
Beta1 [12–16]	11.64384	11.76471	4.31034	9.53347	9.418838	1.02564
Beta2 [16–24]	2.92398	12.5	9.7561	17.1875	7.82123	4.97512
TOT	9.676182	9.7288	9.1022	9.12	9.92351	9.54763

Percent variation for each channel, for each rhythm between the energy of amplitude spectrum of 1-min trace before the EPI sequence, and the energy of amplitude spectrum after the EPI sequence, of biological phantom. The amplitude spectrum was computed by real FFT of 2-s epochs averaging of 1-min traces considered. Note that the percent value of the entire band considered, for each channel, was more or less 9%, so there is not significant variation in energy. It's possible to use the hypothesis that during the EPI sequence, the only contribution of information of electrical signal of phantom wouldn't have substantial changes out of this percent values.

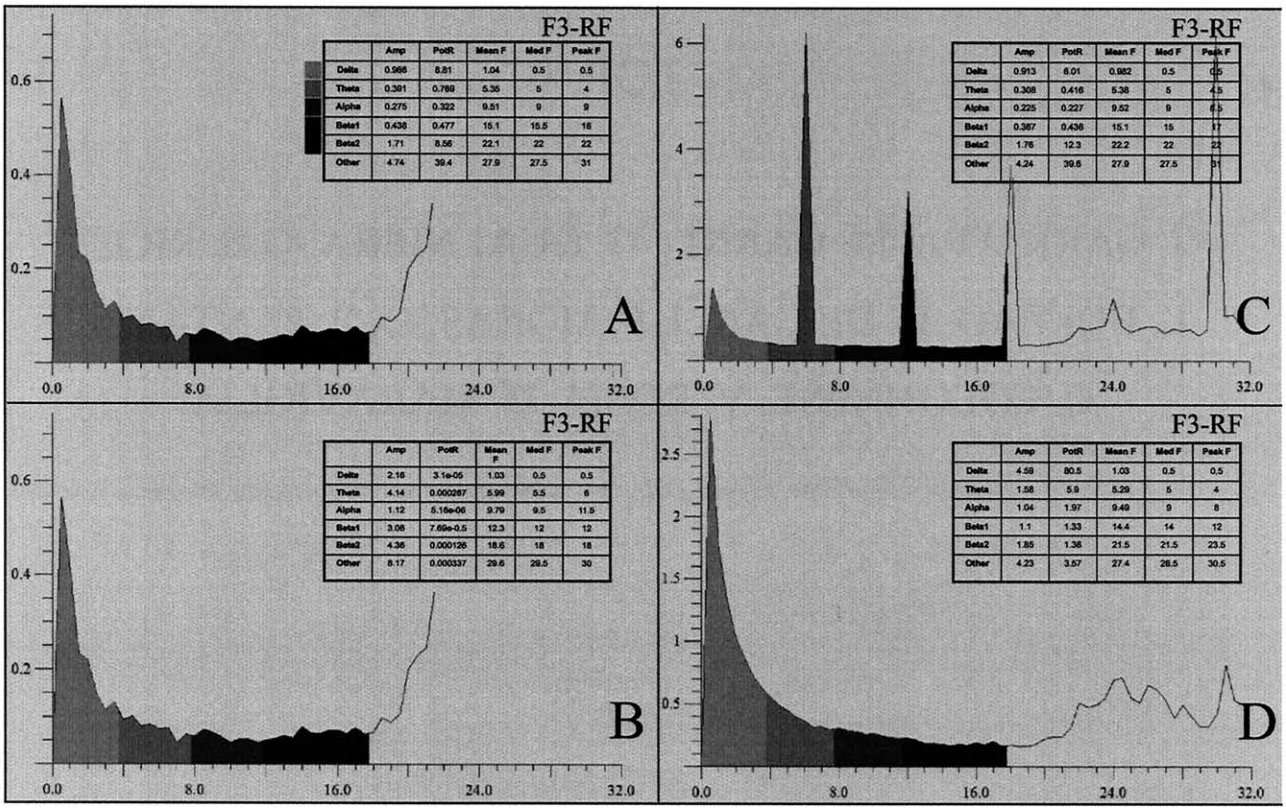

Fig. 7. One-minute amplitude spectrum of one channel recorded of biologic phantom, inside the MR scanner. The amplitude spectrum was computed by average of 2-s epoch FFT signal. Here are represented four different situations recording: (A) before EPI sequence (only static magnetic field effect); (B) after EPI sequence (only static magnetic field effect); (C) during EPI sequence (gradients fields, static magnetic field and RF pulse effects); and (D) during EPI sequence with adaptive filtering.

grapho-elements can be altered either by a consistent reduction or by the disappearance of the seizures activity preventing any fMRI study. In this case it's possible to avoid a loss of time and an useless stress for the patient by stopping the EEG/fMRI acquisition and, in turn, by completing the examination with a better anatomic MRI study.

Regarding these best results, it's confirmed that the nature of the magnetic interference during the EPI sequence is completely known and does not depend properly by the type of objects studied, hence it is possible to obtain similar good results also recording EEG signal of healthy normal subjects and pathologic subjects too. For each of these cases the same EEG/fMRI acquisition protocol was used, and best results were obtained too.

Presented below is the case of one representative healthy subject (volunteer, male, age 30). A specified Real-time artifact reduction algorithm was launched during the EEG/fMRI recording, and after 15 volumes EPI time acquisition (used in order to create and calibrate the artifact model) a completely cleaned EEG without any loss of information was presented also during the recording, making possible to monitor the neuronal activity.

Table 2
Percent variation for each channel: biological phantom during EPI sequence

Band [Hz]	F3	Fz	F4	Cz	P3	P4
Delta [0–4]	8.701923	5.389222	1.234568	25.5102	7.480818	0.320513
Theta [4–8]	29.81928	14.55823	35.43103	15.70048	1.09589	10.81395
Alpha [8–12]	39.32039	63.72549	6.743421	6.218905	13	19.4186
Beta1 [12–16]	17.66467	53.9823	3.947368	9.385965	6.840816	3.921569
Beta2 [16–24]	13.39869	10.11984	7.027027	13.97059	1.639344	2.830189
TOT	7.146446	20.47893	6.611227	15.62288	2.196259	2.445652

Percent variation for each channel, for each rhythm between the energy of amplitude spectrum of 1-min trace out of the EPI sequence (computed by using the average of amplitude spectrum before and after the EPI sequence), and the energy of amplitude spectrum during the EPI sequence (after adaptive filtering), of biological phantom. The amplitude spectrum was computed by real FFT of 2-s epochs averaging of 1-min traces considered. Note that the percent value of the entire band considered, for each channel was more or less 9%, so the hypothesis of range variability was hence confirmed.

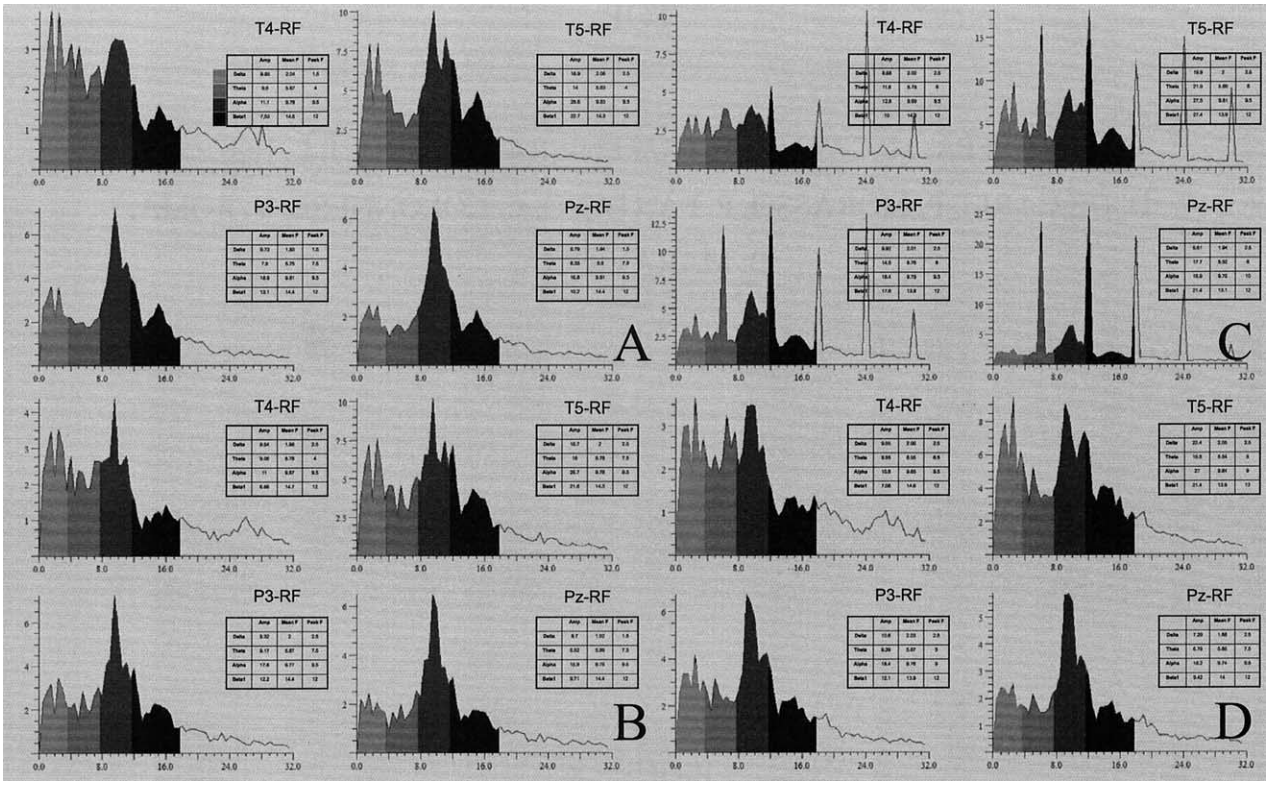

Fig. 8. One-minute amplitude spectrum of four channels recorded of healthy male volunteer patient (age 30) inside the MR scanner. The amplitude spectrum was computed by average of 2-s epoch FFT signal. Here are represented four different situations recording: (A) before EPI sequence (only static magnetic field effect); (B) after EPI sequence (only static magnetic field effect); (C) during EPI sequence (gradient fields, static magnetic field and RF pulse effects); and (D) during EPI sequence with adaptive filtering.

With the same modality used for the biologic phantom, humans studies were performed, the amplitude spectrum inside the MR scanner was computed for 1 min recording of each channel (averaged along 2 s epoch length) in four different situations: before, during and after the EPI sequence, and during the artifact filtering (Fig. 8)

In particular, to the subject we asked to close the eyes for all the duration of recording. In this condition it was found that, in all four situations (Fig. 8), the alpha rhythm ([8-12] Hz bandwidth) is more evident than the other rhythms because the normal EEG activity was substituted by the initial rest state (closed eyes).

The percent variation of the energy of the entire band considered between the "before sequence" to the "after sequence" was around 6.2%, hence the variability obtained was less relevant than the variability computed on the biologic phantom (9%) (Table 3).

$$\text{Percentual Variation function: } Vp_{band}\% = \text{abs}((\mathbf{before}_{band} - \mathbf{after}_{band})/\mathbf{before}_{band}) *100.$$

Similar variability values were obtained between the

Table 3
Percent variation for each channel: male healthy volunteer before and after EPI sequence

Band	Fp1	Fp2	F7	F3	Fz	F4	F8	T3	C3	Cz	C4	T4	T5	P3	Pz	P4	T6	O1	O2
Delta	7.94	12.8	27.59	3.23	9.17	12.61	5.80	2.22	2.96	8.92	21.53	9.30	2.02	5.20	4.20	2.32	1.69	55.72	38.85
Theta	0.00	1.74	5.88	4.53	15.18	2.80	2.08	3.60	11.67	5.13	4.05	1.00	16.43	16.24	11.42	3.79	1.48	34.33	20.48
Alpha	4.48	2.08	4.39	5.91	3.66	3.51	2.26	6.29	3.20	9.85	4.40	0.89	4.70	1.05	1.21	0.55	4.64	4.23	2.27
Beta1	7.04	6.21	6.25	12.94	6.72	10.28	8.99	7.33	8.40	45.57	5.02	0.14	7.11	9.30	6.72	1.92	4.96	21.90	9.09
Beta2	1.10	2.51	0.66	7.38	7.26	6.58	7.05	2.95	10.16	7.28	2.76	3.67	7.59	6.82	5.12	5.17	2.44	26.61	9.63
TOT	3.62	4.99	5.29	2.70	8.34	7.67	4.35	2.46	1.22	11.46	4.27	1.76	1.85	1.85	0.70	0.18	0.88	33.63	20.75

Percent variation for each channel, for each rhythm between the energy of amplitude spectrum of 1-min trace before the EPI sequence, and the energy of amplitude spectrum after the EPI sequence, of 30 aged male healthy volunteer. The amplitude spectrum was computed by real FFT of 2-s epochs averaging of 1-min traces considered. Note that the percent value of the entire band considered, for each channel was more or less 6.2%, so there is not significant variation in energy.

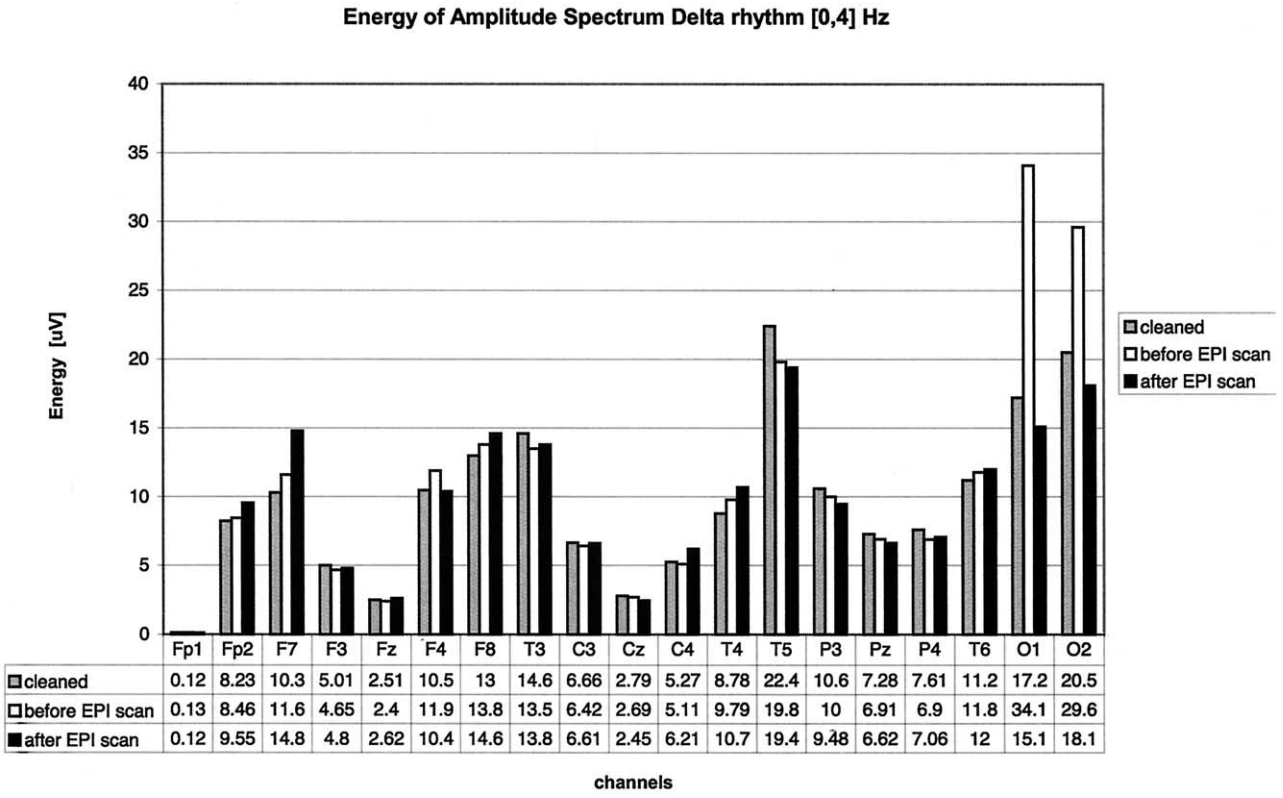

	Fp1	Fp2	F7	F3	Fz	F4	F8	T3	C3	Cz	C4	T4	T5	P3	Pz	P4	T6	O1	O2
cleaned	0.12	8.23	10.3	5.01	2.51	10.5	13	14.6	6.66	2.79	5.27	8.78	22.4	10.6	7.28	7.61	11.2	17.2	20.5
before EPI scan	0.13	8.46	11.6	4.65	2.4	11.9	13.8	13.5	6.42	2.69	5.11	9.79	19.8	10	6.91	6.9	11.8	34.1	29.6
after EPI scan	0.12	9.55	14.8	4.8	2.62	10.4	14.6	13.8	6.61	2.45	6.21	10.7	19.4	9.48	6.62	7.06	12	15.1	18.1

Fig. 9. Bar plot of energy computed for each channel recorded from the amplitude spectrum, in three different cases, related to delta rhythm (0-4) Hz. Note that there is no substantial variability before, during (with artifact reduction), and after the EPI sequence.

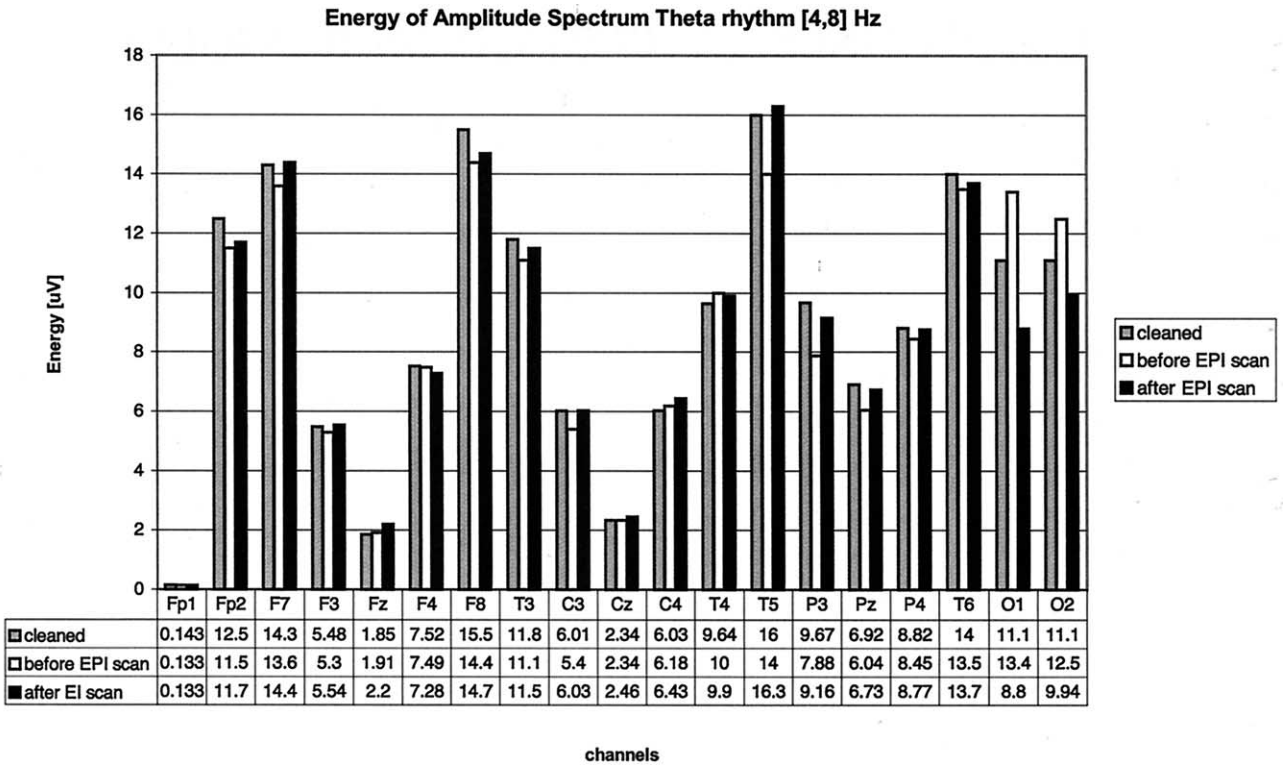

	Fp1	Fp2	F7	F3	Fz	F4	F8	T3	C3	Cz	C4	T4	T5	P3	Pz	P4	T6	O1	O2
cleaned	0.143	12.5	14.3	5.48	1.85	7.52	15.5	11.8	6.01	2.34	6.03	9.64	16	9.67	6.92	8.82	14	11.1	11.1
before EPI scan	0.133	11.5	13.6	5.3	1.91	7.49	14.4	11.1	5.4	2.34	6.18	10	14	7.88	6.04	8.45	13.5	13.4	12.5
after EI scan	0.133	11.7	14.4	5.54	2.2	7.28	14.7	11.5	6.03	2.46	6.43	9.9	16.3	9.16	6.73	8.77	13.7	8.8	9.94

Fig. 10. Bar plot of energy computed for each channel recorded from the amplitude spectrum, in three different cases, related to theta rhythm (4-8) Hz. Note that there is no substantial variability before, during (with artifact reduction) and after the EPI sequence.

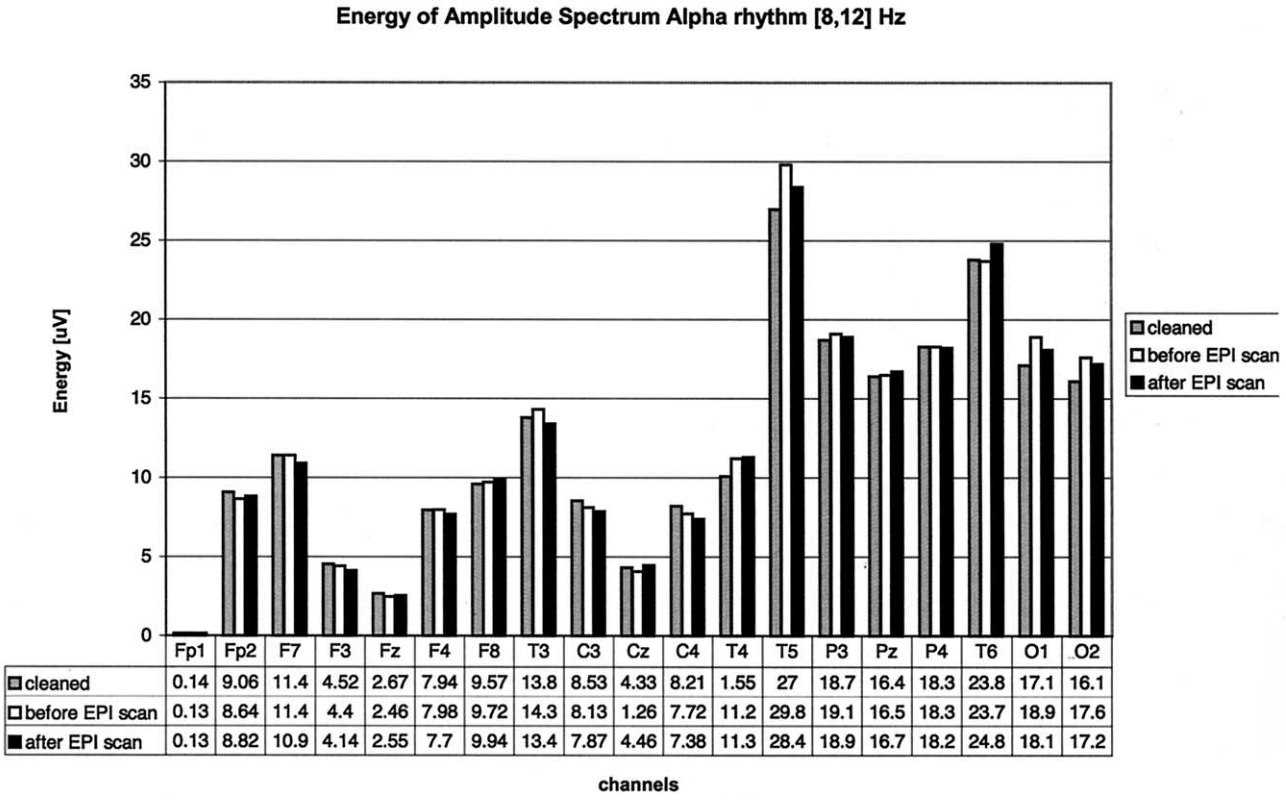

	Fp1	Fp2	F7	F3	Fz	F4	F8	T3	C3	Cz	C4	T4	T5	P3	Pz	P4	T6	O1	O2
cleaned	0.14	9.06	11.4	4.52	2.67	7.94	9.57	13.8	8.53	4.33	8.21	1.55	27	18.7	16.4	18.3	23.8	17.1	16.1
before EPI scan	0.13	8.64	11.4	4.4	2.46	7.98	9.72	14.3	8.13	1.26	7.72	11.2	29.8	19.1	16.5	18.3	23.7	18.9	17.6
after EPI scan	0.13	8.82	10.9	4.14	2.55	7.7	9.94	13.4	7.87	4.46	7.38	11.3	28.4	18.9	16.7	18.2	24.8	18.1	17.2

Fig. 11. Bar plot of energy computed for each channel recorded from the amplitude spectrum, in three different cases, related to alpha rhythm (8-12) Hz. Note that there is no substantial variability before, during (with artifact reduction), and after the EPI sequence.

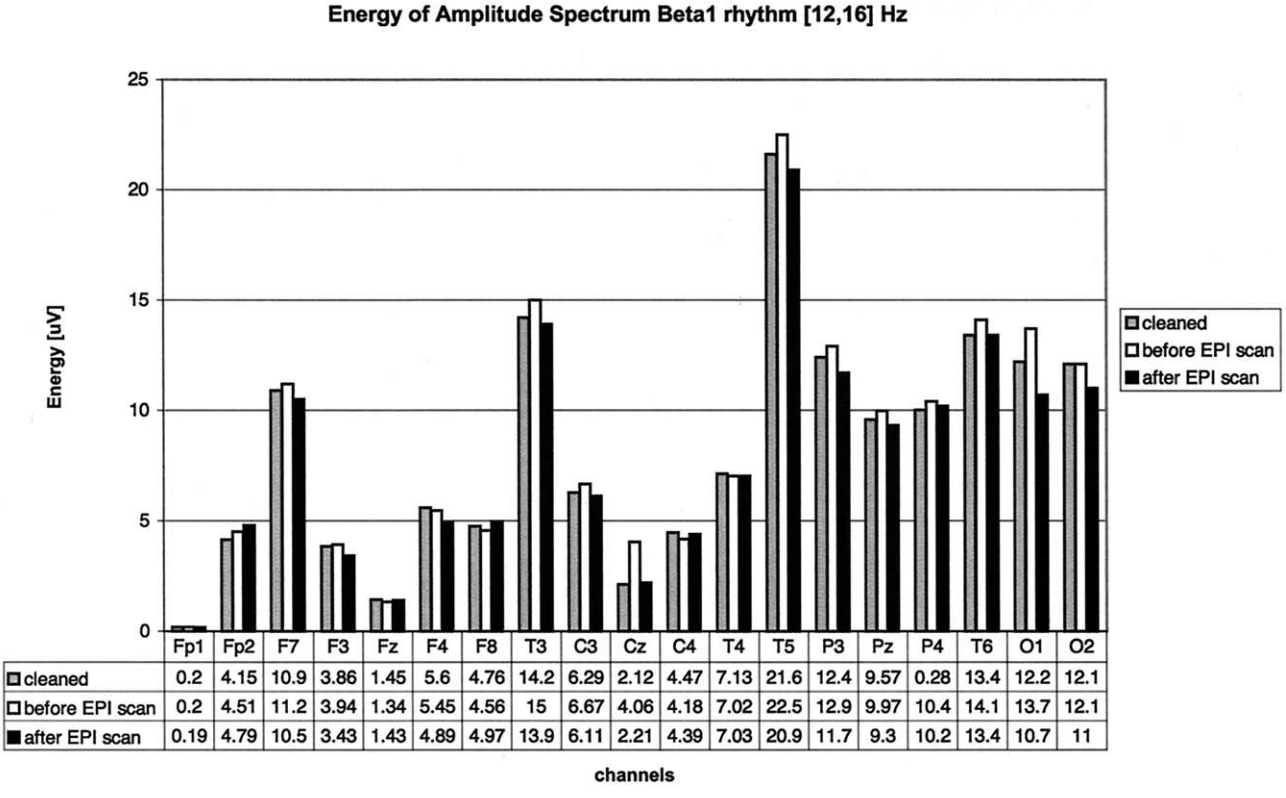

	Fp1	Fp2	F7	F3	Fz	F4	F8	T3	C3	Cz	C4	T4	T5	P3	Pz	P4	T6	O1	O2
cleaned	0.2	4.15	10.9	3.86	1.45	5.6	4.76	14.2	6.29	2.12	4.47	7.13	21.6	12.4	9.57	0.28	13.4	12.2	12.1
before EPI scan	0.2	4.51	11.2	3.94	1.34	5.45	4.56	15	6.67	4.06	4.18	7.02	22.5	12.9	9.97	10.4	14.1	13.7	12.1
after EPI scan	0.19	4.79	10.5	3.43	1.43	4.89	4.97	13.9	6.11	2.21	4.39	7.03	20.9	11.7	9.3	10.2	13.4	10.7	11

Fig. 12. Bar plot of energy computed for each channel recorded from the amplitude spectrum, in three different cases, related to beta1 rhythm (12-16) Hz. Note that there is no substantial variability before, during (with artifact reduction), and after the EPI sequence.

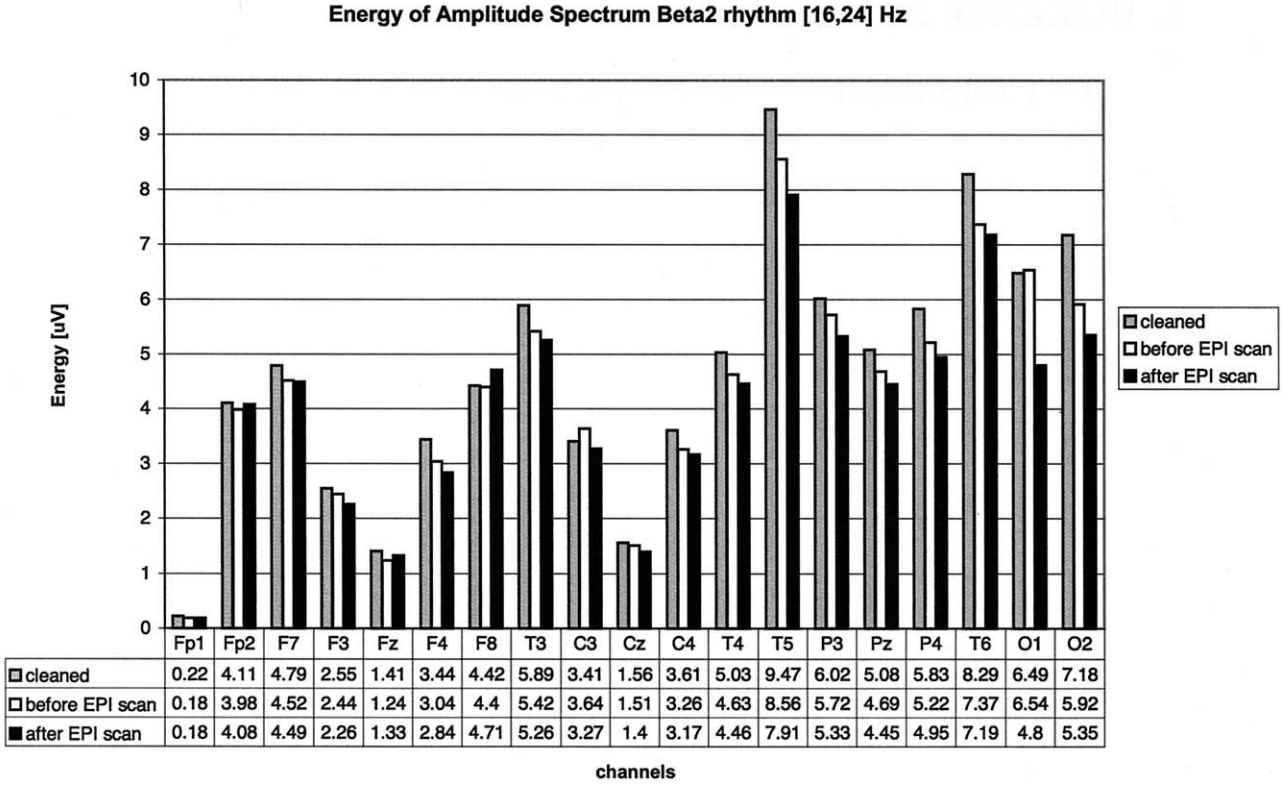

	Fp1	Fp2	F7	F3	Fz	F4	F8	T3	C3	Cz	C4	T4	T5	P3	Pz	P4	T6	O1	O2
cleaned	0.22	4.11	4.79	2.55	1.41	3.44	4.42	5.89	3.41	1.56	3.61	5.03	9.47	6.02	5.08	5.83	8.29	6.49	7.18
before EPI scan	0.18	3.98	4.52	2.44	1.24	3.04	4.4	5.42	3.64	1.51	3.26	4.63	8.56	5.72	4.69	5.22	7.37	6.54	5.92
after EPI scan	0.18	4.08	4.49	2.26	1.33	2.84	4.71	5.26	3.27	1.4	3.17	4.46	7.91	5.33	4.45	4.95	7.19	4.8	5.35

Fig. 13. Bar plot of energy computed for each channel recorded from the amplitude spectrum, in three different cases, related to beta2 rhythm (16-24) Hz. Note that there is no substantial variability before, during (with artifact reduction), and after the EPI sequence.

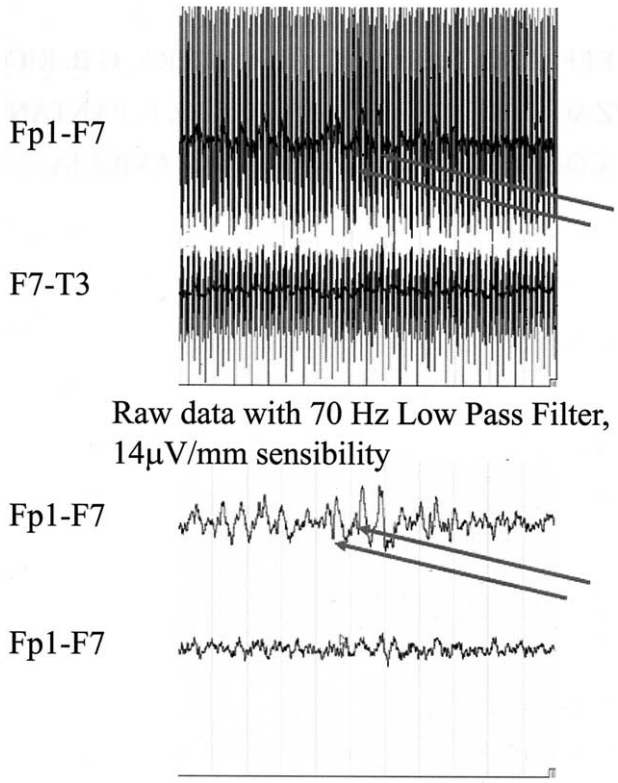

Fig. 14. Particular of EEG acquisition of epileptic patient before, during, and after the MRI scanning. The morphology and the amplitude of the spike activity during the MRI sequence is not changed in respect to the before and after EPI recording

"before/after" sequence and the "cleaned" sequence, shown as follows (Figs. 9-13).

4. Conclusions

It has been proven that it is possible—in real-time mode—to remove quite completely the effects due to the magnetic fields of the EPI sequence during simultaneous EEG/fMRI acquisitions.

Best results were obtained during the time and frequency domain validation, noting that there is no loss of information for each channel and for each band considered, and no variation in the shapes and amplitude of the traces. The real-time filtering allows us to directly monitor the EEG and the patient behavior during the EPI acquisition.

In particular, the on-line filtering described above allows clinicians to constantly monitor the patient during fMRI, and we retain this very important for pathologic subjects. Moreover, this becomes useful when the patient does not show a suitable activity for fMRI study. In this case, it is possible to avoid useless stress for the patient and a loss of time and, for example, defer the EEG/fMRI acquisition. Concluding, real-time filtering combined with an optimal EPI protocol, does not modify the morphology and the amplitude of previous EEG activity (Fig. 14). In order to verify this, a study was performed on three pathologic subjects, and representative results were summarized in Fig.

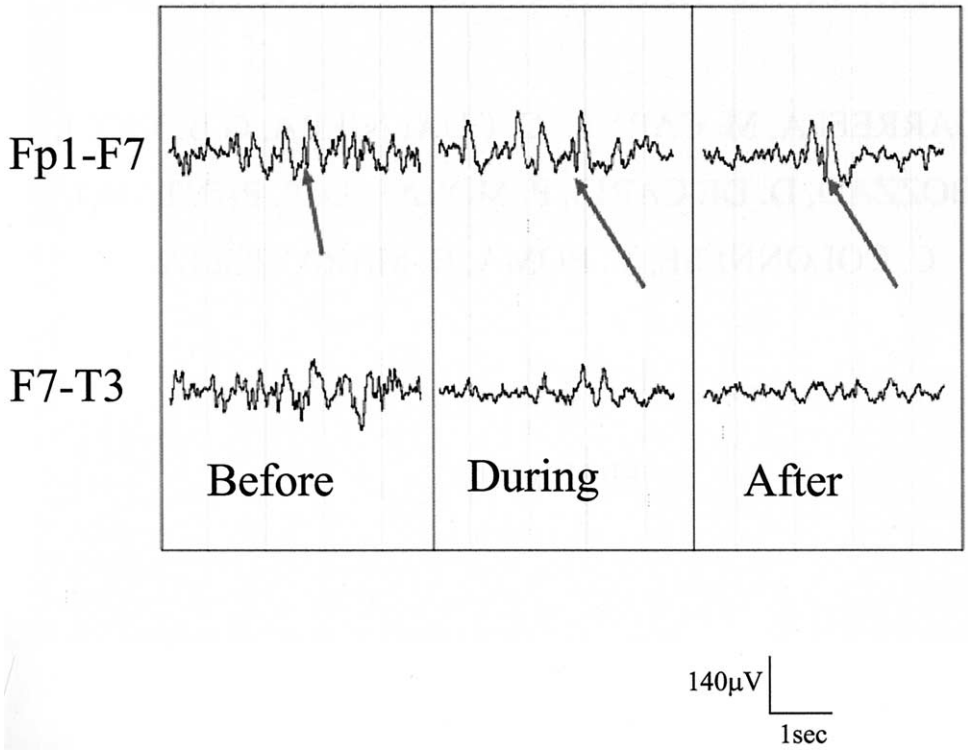

Fig. 15. Effects of the real-time filtering during the EPI sequence

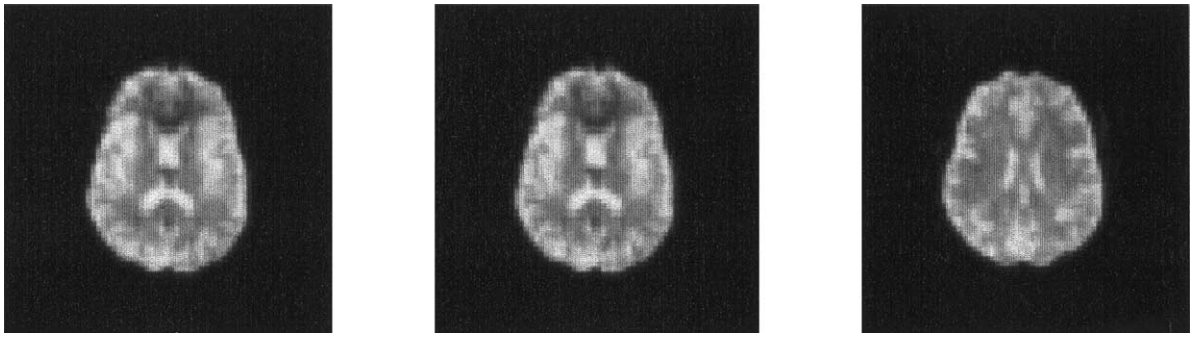

Fig. 16. Example of EPI images acquired during EEG recording (matrix 64 × 64).

15. Furthermore, with our setting, EPI images were of good quality without distortion, signal loss and noise induced from EEG devices (Fig. 16).

Fig. 15 shows a detail of an EEG acquisition of an epileptic patient before, during and after the MRI scanning. The morphology and the amplitude of the spike activity during the MRI sequence is not changed with respect to the before and after EPI recording.

The on-line acquisition here can be also applied to acquisition of evoked potentials or study of cerebral rhythms (for instance alpha rhythm).

Acknowledgments

The authors acknowledge the support of Walter Nucciarelli at the Department of Neurologic Sciences, University of Rome, La Sapienza, Italy.

References

[1] Warach S, Ives JR, Schlaug G, Patel MR, Darby DG, Thangaraj V, Edelman RR, Schomer DL. EEG-triggered echo-planar functional MRI in epilepsy. Neurology 1996;47:89–3.

[2] Ives JR, Warach S, Schmitt F, Edelman RR, Schomer DL. Monitoring the patient's EEG during echo planar MRI. Electroencephalogr Clin Neurophysiol 1993;87:417–20.

[3] Allen PJ, Polizzi G, Krakow K, Fish DR, Lemieux L. Identification of EEG events in the MR scanner: the problem of pulse artifact and a method for its subtraction. Neuroimage 1998;8:229–39.

[4] Krakow K, Woermann FG, Symms MR, Allen PJ, Lemieux L, Barker GJ, Duncan JS, Fish DR. EEG-triggered functional MRI of interictal epileptiform activity in patients with partial seizures. Brain 1999;122: 1679–88.

[5] Allen PJ, Josephs O, Turner R. A method for removing artifact from continuous EEG recorded during functional MRI. Neuroimage 2000; 12:230–9.

[6] Huang-Hellinger FR, Breiter CH, McCormark G, Cohen MS, Kwong KK, Sutton JP, Savoy RL, Weisskoff RM, Davis TL, Baker JR,

Belliveau JW, Rosen BR. Simultaneous functional magnetic resonance imaging and electrophysiological recording. Hum Brain Mapping 1995;3:13–23.

[7] Lemieux L, Allen PJ, Franconi F, Symms MR, Fish DR. Recording of EEG during fMRI experiments: patient safety. Magn Reson Med 1997;38:943–52.

[8] Hoffmann A, Jäger L, Werhahn KJ, Jaschke M, Noachtar S, Reiser M. Electroencephalography during functional echo-planar imaging: detection of epileptic spikes using post-processing methods. Magn Reson Med 2000;44:791–8.

[9] Bénar CG, Aghakhani Y, Wang Y, Izenberg A, Al-Asmi A, Dubeau F, Gotman J. Quality of EEG in simultaneous EEG-fMRI for epilepsy. Clin Neurophysiol 2003;114:569–80.

[10] Goldman RI, Stern JM, Engel J, Cohen MS. Acquiring simultaneous EEG and functional MRI. Clin Neurophysiol 2000;111:1974–80.

[11] Baumann SB, Noll DC. A modified electrode cap for EEG recordings in MRI scanners. Clin Neurophysiol 1999;110:2189–93.

[12] Strobach P, Klaus A-F, Härer W. Event-synchronous cancellation of the heart interference in biomedical signals. IEEE Trans Biomed Engineer 1994;41:343–50.